processes

MDPI

Article

Mg/Fe Layered Double Hydroxide Modified Biochar for Synergistic Removal of Phosphate and Ammonia Nitrogen from Chicken Farm Wastewater: Adsorption Performance and Mechanisms

Tao Li [1,2,3,4], Jinping Li [1,3,4,*], Zengpeng Li [2] and Xiuwen Cheng [5]

[1] School of Energy and Power Engineering, Lanzhou University of Technology, Lanzhou 730050, China; litaolichun@163.com
[2] School of Bioengineering, Jiuquan Vocational Technical University, Jiuquan 735300, China; lzpjqzy@163.com
[3] Collaborative Innovation Center for Supporting Technology of Northwest Low-Carbon Towns, Lanzhou 730050, China
[4] Gansu Key Laboratory of Complementary Energy System of Biomass and Solar Energy, Lanzhou 730050, China
[5] College of Earth and Environmental Sciences, Lanzhou University, Lanzhou 730050, China; chengxw@lzu.edu.cn
* Correspondence: lijinping77@163.com; Tel.: +86-13919773347

Abstract

The development of an economical and efficient method for recovering phosphate (PO_4^{3-}-P) and ammonium nitrogen (NH_4^+-N) is of paramount importance for environmental remediation. The preparation of Mg/Fe-loaded biochar (Mg/Fe-BC) was achieved through chemical precipitation followed by pyrolysis in this study. Single solution adsorption studies indicated that temperature significantly affected how effectively Mg/Fe-BC could adsorb and remove NH_4^+-N, whereas PO_4^{3-}-P adsorption showed minimal temperature sensitivity. In mixed simulated solutions, In the mixed simulated solution, the maximum adsorption capacities of Mg/Fe-BC for PO_4^{3-}-P and NH_4^+-N were 145.97–153.05 mg/g and 112.63–121.51 mg/g, respectively. The optimal dosage for synergistic adsorption was determined to be 3 g/L, while pH values ranging from 3 to 9 exhibited negligible effects on the adsorption of both contaminants. The presence of Ca^{2+} and HCO_3^- in the solution may interfere with the simultaneous adsorption of PO_4^{3-}-P and NH_4^+-N. SEM-EDS and XPS analyses revealed that the primary adsorption mechanisms of PO_4^{3-}-P and NH_4^+-N by Mg/Fe-BC involved electrostatic attraction, ion exchange, and hydrogen bonding. In practical applications using chicken manure biogas slurry, Mg/Fe-BC demonstrated synergistic adsorption effects, achieving removal efficiencies of 86.86% for PO_4^{3-}-P and 36.86% for NH_4^+-N, thereby confirming its potential application value in wastewater treatment.

Keywords: modified biochar; adsorption capacity; removal rate; chemical adsorption

check for updates

Academic Editor: Federica Raganati

Received: 15 July 2025
Revised: 3 August 2025
Accepted: 5 August 2025
Published: 8 August 2025

Citation: Li, T.; Li, J.; Li, Z.; Cheng, X. Mg/Fe Layered Double Hydroxide Modified Biochar for Synergistic Removal of Phosphate and Ammonia Nitrogen from Chicken Farm Wastewater: Adsorption Performance and Mechanisms. *Processes* **2025**, *13*, 2504. https://doi.org/10.3390/pr13082504

Copyright: © 2025 by the authors. Licensee MDPI, Basel, Switzerland. This article is an open access article distributed under the terms and conditions of the Creative Commons Attribution (CC BY) license (https://creativecommons.org/licenses/by/4.0/).

1. Introduction

With the rapid expansion of global poultry and livestock industries, the substantial amounts of manure and other waste generated by large-scale farms pose significant threats to ecological environments [1,2]. In China, annual production from over 500 million pigs and 10 billion poultry creates massive quantities of manure, representing a major environmental challenge [3]. Livestock manure contains high concentrations of nutrients such

as phosphorus (P) and nitrogen (N), which can be released into water bodies through slurry discharge, leading to ecological issues including water eutrophication and algal blooms [1,4]. Anaerobic digestion has been widely adopted as an effective method for treating livestock manure, demonstrating multiple benefits including organic pollutant removal, odor control, nutrient recovery, and pathogen reduction, while simultaneously producing valuable renewable energy in the form of biogas [5,6]. According to Duan et al. [7], approximately 90% of biogas plants in China were constructed specifically for manure management to enhance pollution control of waste materials. Although conventional anaerobic digestion converts organic phosphorus and nitrogen into phosphate and ammonia, the process generates substantial amounts of biogas slurry containing high concentrations of ammonia nitrogen (90–8000 mg/L) and phosphate (7–381 mg/L) [8,9]. Direct application of this nutrient-rich wastewater to soil presents environmental safety risks, necessitating further treatment to meet discharge standards.

To address these environmental challenges, researchers have employed various methods for recovering phosphate (PO_4^{3-}-P) and ammonium nitrogen (NH_4^+-N) from wastewater, including membrane filtration, chemical precipitation, biological treatment, and adsorption [10]. However, the large-scale application of membrane filtration is constrained by pore clogging issues and high operational costs [11], while chemical precipitation requires additional chemical reagents and prolonged reaction time, making it economically and environmentally unsustainable [12]. In recent years, biochar has emerged as a cost-effective biomaterial for recovering organic pollutants and nutrients from agricultural and industrial wastewater. Previous studies mainly focused on utilizing the oxygen-containing functional groups or negatively charged groups on the surface of biochar to enhance the electrostatic interaction and attract NH_4^+ [13]. Nevertheless, pristine biochar exhibits limited adsorption capacity for PO_4^{3-}-P and NH_4^+-N. Consequently, metal ion co-precipitation modification has gained significant attention due to its low cost and high efficiency, and it has been shown to significantly enhance the adsorption performance of biochar for PO_4^{3-}-P and NH_4^+-N [14,15]. These metal-loaded biochars demonstrate improved pollutant removal efficiency, offering a promising solution for sustainable wastewater treatment.

Layered double hydroxides (LDHs), as novel and environmentally friendly materials for phosphorus removal from wastewater, possess positively charged layered mixed hydroxide structures that readily undergo anion exchange with phosphates, endowing them with excellent adsorption capacity for anionic pollutants [16]. Loading LDHs onto eco-friendly biochar (BC) can enhance their dispersion and stability, while in turn, LDHs significantly improve the ion exchange capacity of BC [17]. Previous studies have reported that magnetic biochar exhibits high affinity for phosphates and offers the distinct advantage of easy separation after phosphorus recovery [18]. Magnesium-modified biomass not only enables simultaneous adsorption of P and N from aqueous solutions but also allows the nutrient-loaded adsorbent to be repurposed as agricultural fertilizer due to its environmentally benign characteristics [19]. The introduction of magnesium ions primarily facilitates the formation of struvite from phosphate and ammonium, thereby maximizing the utilization efficiency of LDH-BC in wastewater treatment.

Based on this foundation, the present study employed a co-precipitation approach using magnesium and iron metal salts with waste biomass, followed by pyrolysis technology to firmly couple LDHs onto pristine BC. The resulting composite material possesses the adsorption characteristics of biochar porous media as well as the superior performance of chemical reactions such as ion exchange. The synthesized composite demonstrated exceptional synergistic adsorption performance for components in poultry farm wastewater. This research systematically investigated: (1) the adsorption process and removal efficiency of PO_4^{3-}-P and NH_4^+-N in solution by Mg/Fe-BC; (2) the underlying adsorption

mechanisms; and (3) the adsorption behavior of Mg/Fe-BC in chicken manure biogas slurry mixtures. This study aims to provide potential application strategies for recovering PO_4^{3-}-P and NH_4^+-N from poultry farm wastewater.

2. Materials and Methods

2.1. Chemicals and Raw Materials

The chemical reagents ($MgCl_2 \cdot 6H_2O$, $FeCl_3 \cdot 6H_2O$, NaOH, KH_2PO_4, and NH_4Cl) were purchased from Tianjin Kemiou Chemical Reagent Co., Ltd (Tianjin, China). For biomass preparation, fresh corn cobs collected from Jiuquan (China) were naturally air-dried, cleaned of impurities, milled to pass a 100-mesh sieve, and preserved in a desiccator. The chicken manure-derived biogas slurry was obtained from a separate farm in the same region. The concentrations of soluble chemical oxygen demand (SCOD), total nitrogen (TN), PO_4^{3-}-P, and NH_4^+-N in the biogas slurry are presented in Table 1.

Table 1. Composition of liquid chicken manure biogas slurry.

Parameter	pH	SCOD (mg/L)	TN (mg/L)	NH_4^+-N (mg/L)	PO_4^{3-}-P (mg/L)
Biogas slurry	8.16	3067.84	2466.57	1279.45	32.86

2.2. Preparation of Modified Biochar

The Mg/Fe-BC was prepared according to a modified Bian et al. method [20]. Corn cob biomass (50 g) was soaked in 500 mL of 0.2 mol/L $FeCl_3 \cdot 6H_2O$ and 0.4 mol/L $MgCl_2 \cdot 6H_2O$ mixed solution, and then ultrasonicated (30 min, RT) for uniform metal dispersion. After pH adjustment to 10 (2.5 mol/L NaOH), the mixture was aged (60 °C, 12 h), filtered, washed (DI water × 3), and dried (60 °C, 24 h). Pyrolysis was conducted in N_2 atmosphere (200 mL/min) at 500 °C (2 h, 10 °C/min ramp). The cooled product was stored in an airtight container. Under the same conditions, the unmodified BC was used as the control.

2.3. Characterization and Analysis

The surface morphology and elemental composition of the modified biochar were characterized using scanning electron microscopy (SEM, Gemini SEM 500, Oberkochen, Germany) coupled with energy-dispersive X-ray spectroscopy (EDS, Oxford Ultim Max 100, Oxford, UK). Surface charge properties were determined via zeta potential measurements (Zetasizer Nano ZS 90, Malvern, UK). Material physical properties were analyzed by Brunauer-Emmett-Teller (BET) surface area analysis (Micromeritics ASAP 2420, Norcross, GA, USA). Crystalline structures were examined using X-ray diffraction (XRD, Bruker D8 Discover, Karlsruhe, Germany), while functional group composition was identified through Fourier-transform infrared spectroscopy (FTIR, Nicolet iS5, Waltham, MA, USA). Chemical states were further investigated by X-ray photoelectron spectroscopy (XPS, Thermo Scientific K-Alpha, Waltham, MA, USA).

2.4. Batch Adsorption Experiments

A mixed solution containing PO_4^{3-}-P and NH_4^+-N was prepared using NH_4Cl and KH_2PO_4. For each test, 0.1 g of Mg/Fe-BC was added to 100 mL of the mixed solution containing 120 mg/L of both PO_4^{3-}-P and NH_4^+-N. The mixture was shaken at 150 rpm in a thermostatic oscillator at 25 °C for 24 h, and then filtered through a 0.45 μm membrane for analysis. The phosphorus content was determined using the ammonium molybdate spectrophotometric method, while the nitrogen content was measured by Nessler's reagent spectrophotometry, with all treatments performed in triplicate. For single-component adsorption tests, only PO_4^{3-}-P or NH_4^+-N solutions were used, while maintaining identical

experimental conditions [20,21]. The initial concentration of the mixed solution remained the same. The impact of varying initial pH (2–10) and the presence of competing ions on PO_4^{3-}-P and NH_4^+-N adsorption was comprehensively analyzed. The experiment also investigated the effects of the dosage of Mg/Fe-BC (0.5–5 g/L) on the adsorption equilibrium capacity and removal rate of PO_4^{3-}-P and NH_4^+-N. Refer to Text S1 for the formulas calculating the equilibrium adsorption capacity and removal rate of PO_4^{3-}-P and NH_4^+-N.

Samples were collected at 5, 10, 15, 30, 60, 120, 240, 480, 720, and 1440 min to determine PO_4^{3-}-P or NH_4^+-N concentrations in the filtrate for adsorption kinetic studies. The detailed equations of the pseudo-first-order model and the pseudo-second-order model are presented in Text S2. Adsorption isotherm analysis was conducted at 25 °C, 35 °C, and 45 °C with varying initial concentrations (40, 60, 80, 120, 160, 200, 240, 280, and 320 mg/L for both PO_4^{3-}-P and NH_4^+-N) to thoroughly investigate the adsorption behavior and characteristics. The equations of the Langmuir model and the Freundlich model are shown in Text S3. The adsorption performance of Mg/Fe-BC (3–30 g/L) for PO_4^{3-}-P and NH_4^+-N was evaluated in real chicken manure biogas slurry. The influence of contact time on adsorption capacity is consistent with the previous kinetic research method.

2.5. Adsorption Regeneration Experiment

A cyclic adsorption experiment was conducted by adding 30 g/L Mg/Fe-BC to 100 mL of chicken manure biogas slurry. After reaching equilibrium, the Mg/Fe-BC was filtered out and desorbed with ammonia water at 25 °C and 150 r/min for 12 h. The adsorption material was collected using a 0.45 μm filter membrane and used for the next cycle experiment. Both PO_4^{3-}-P and NH_4^+-N levels were analyzed by the same methodology, and all cyclic tests were conducted in triplicate.

2.6. Data Analysis

Statistical analysis was performed using Microsoft Office Excel, and data visualization was conducted using Origin Pro 2021.

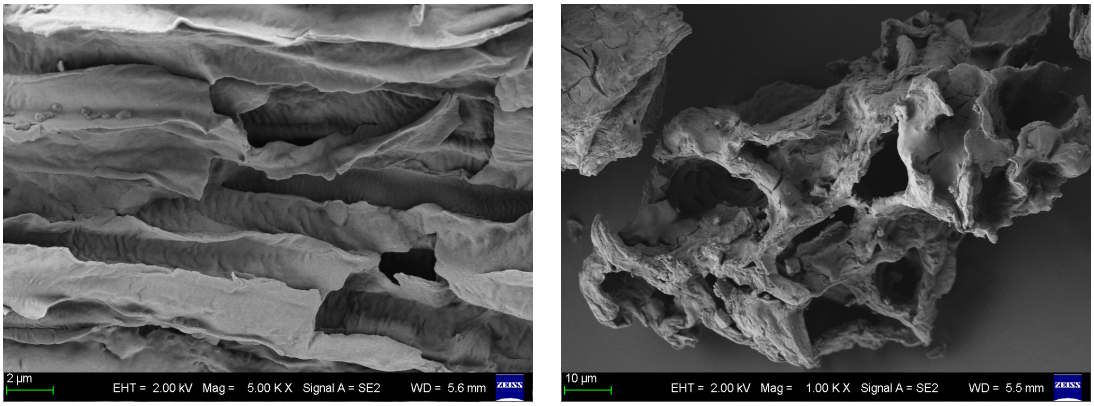
3. Results and Discussion

3.1. Characterization of Composite Materials

SEM analysis revealed distinct morphological differences between BC and Mg/Fe-BC (Figure 1). The surface of BC appears relatively smooth, with a large number of folds distributed on it. Most of the pore channels have a tubular structure, and the pore wall structure is overlapped. After modification, the morphological characteristics of Mg/Fe-BC are quite different. The roughness of the surface structure increases, and many pores are covered with a large number of metal oxide particles [22]. Most of the deposits are clustered. This indicates that the biochar has successfully combined with magnesium and iron metal oxides. This metal loading can increase the density of surface adsorption active sites. Moreover, Mg/Fe-BC has abundant multi-level pore structures. This multi-scale pore network can provide sufficient diffusion channels and adsorption sites for the adsorption of pollutants [23].

The comparative analysis in Table 2 indicates that the modification process considerably improved the specific surface area (71.69 m^2/g) and pore volume (0.1574 cm^3/g) of Mg/Fe-BC over BC. This was attributed to the deposition of metal oxides, which made the surface of Mg/Fe-BC rougher and the pore structure richer. These irregular and uneven pores are beneficial for the adsorption of pollutants [24]. Chemical precipitation and pyrolysis gave rise to the development of the pore structure of Mg/Fe-BC. Although the pore diameter of Mg/Fe-BC slightly decreased (9.35 nm), the diameter still remained within the

mesoporous range (2–50 nm) because the presence of mesopores promoted the effective diffusion and transport of the adsorbent within the carbon matrix [25].



(**a**) (**b**)

Figure 1. SEM images of BC (**a**) and Mg/Fe-BC (**b**).

Table 2. The physicochemical properties of two types of biochar materials.

Sample	BET (m^2/g)	Pore Volume (cm^3/g)	Pore Diameter (nm)	Productivity (%)
BC	3.43	0.0134	13.92	35.17
Mg/Fe-BC	71.69	0.1574	9.35	58.12

The XRD patterns of both Mg/Fe-BC and BC are presented in Figure 2a. The characteristic peaks observed at 18.39°, 35.53°, 53.36°, and 56.95° are Mg/Fe-LDH, indicating that the combined modification of magnesium and iron led to the formation of LDHs [26,27]. The sharp peaks at 31.82° and 45.51° are NaCl, and the weak characteristic peaks at 28.38° and 40.53° are KCl. The KCl diffraction peaks in Mg/Fe-BC gradually disappeared, which might be related to the coverage of metal oxides [27]. The diffraction peaks at 30.8° and 62.45° are Fe_3O_4, while no such peaks were observed in BC, indicating that the iron was successfully loaded onto BC [25]. At 62.16°, 73.95°, and 77.98°, the characteristic peaks are mainly attributed to the formation of MgO, and magnesium was also successfully bound on BC [14,27,28]. BC anchored the layered double hydrogen metal oxides, providing sufficient adsorption sites for the adsorption of phosphate and ammonia nitrogen. The FTIR spectrum (Figure 2b) also further confirmed the changes in functional groups. The absorption peak at 560–580 cm^{-1} is mainly attributed to the formation of Mg-O and Fe-O, which is consistent with the results in the XRD spectrum. A broad absorption peak at 3400 cm^{-1} of Mg/Fe-BC is related to -OH. The characteristic peaks in the range of 1449–1560 cm^{-1} are mainly the formation of C=C, and the peaks at 1160 cm^{-1} and 1599 cm^{-1} are the characteristic peaks of C-O and COO^- functional groups [17,29,30]. After modification, the increase in carboxyl and phenolic hydroxyl groups is conducive to the adsorption of ammonia nitrogen, and the presence of metal ions promotes the adsorption of phosphate. Compared with the fully positively charged LDH, the zeta potential of Mg/Fe-BC was significantly reduced (Figure 2c). When the pH exceeded 8.91, the surface of Mg/Fe-BC carried a negative charge. Due to the alkaline nature of the biogas slurry, this condition was favorable for the adsorption of NH_4^+. Additionally, the hydroxyl and carboxyl groups of Mg/Fe-BC also had acid-base buffering capacity.

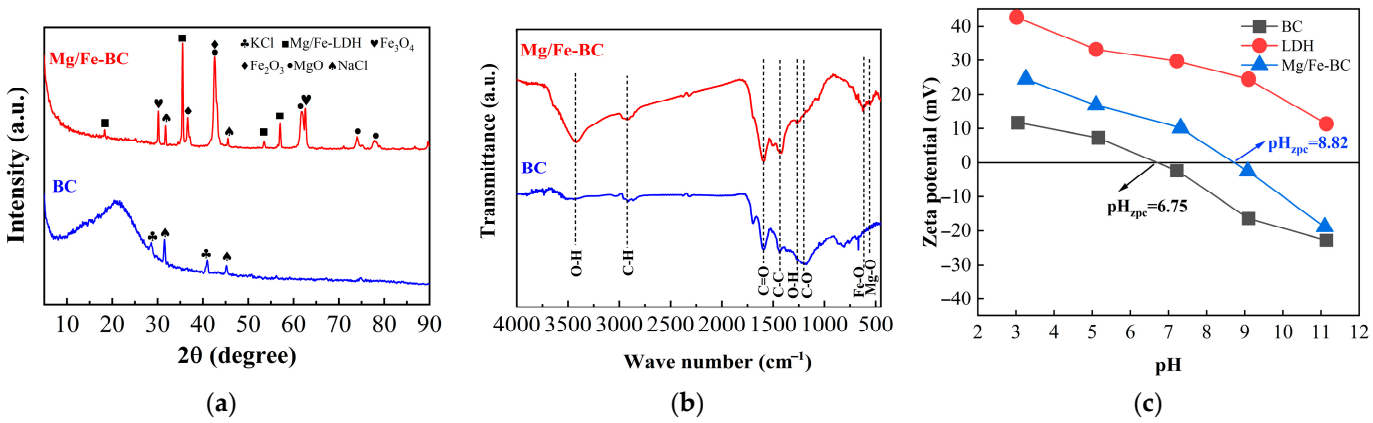


Figure 2. Characterization of Mg/Fe-BC: (**a**) XRD pattern, (**b**) FTIR spectrum, and (**c**) zeta potential.

3.2. The Adsorption Performance of Mg/Fe-BC for PO_4^{3-}-P and NH_4^+-N in a Single Aqueous Solution

As shown in Figure 3, the single-solute adsorption properties of BC and Mg/Fe-BC for either PO_4^{3-}-P or NH_4^+-N were investigated under different temperature conditions. At 25 °C, Mg/Fe-BC exhibited a phosphorus adsorption capacity of 55.03 mg/g in PO_4^{3-}-P solution, representing a 3.4-fold enhancement over pristine BC (16.11 mg/g). Elevating the solution temperature resulted in a progressive increase in PO_4^{3-}-P adsorption by Mg/Fe-BC, ultimately achieving 68.68 mg/g. This result demonstrated that temperature significantly influenced phosphate adsorption by Mg/Fe-BC, which aligned with previous research findings [31]. However, the increase in PO_4^{3-}-P adsorption capacity for BC was less pronounced, primarily due to its limited adsorption capability and insufficient binding sites. Similarly, the phosphorus removal efficiency followed an analogous trend, with the PO_4^{3-}-P removal rate by Mg/Fe-BC increasing at higher temperatures, reaching 57.23% at 45 °C. In the NH_4^+-N single solution, when the temperature increased from 25 °C to 45 °C, the NH_4^+-N adsorption capacity of Mg/Fe-BC rose from 25.03 mg/g to 35.68 mg/g, representing an increase of approximately 42.5%. Compared to BC's adsorption of NH_4^+-N, temperature exhibited a more pronounced effect on the adsorption capacity of Mg/Fe-BC. However, the NH_4^+-N removal rate by Mg/Fe-BC appeared largely unaffected by the increasing ambient temperature, showing only a marginal increase from 26.69% to 29.73%. This variation was even more negligible for BC.

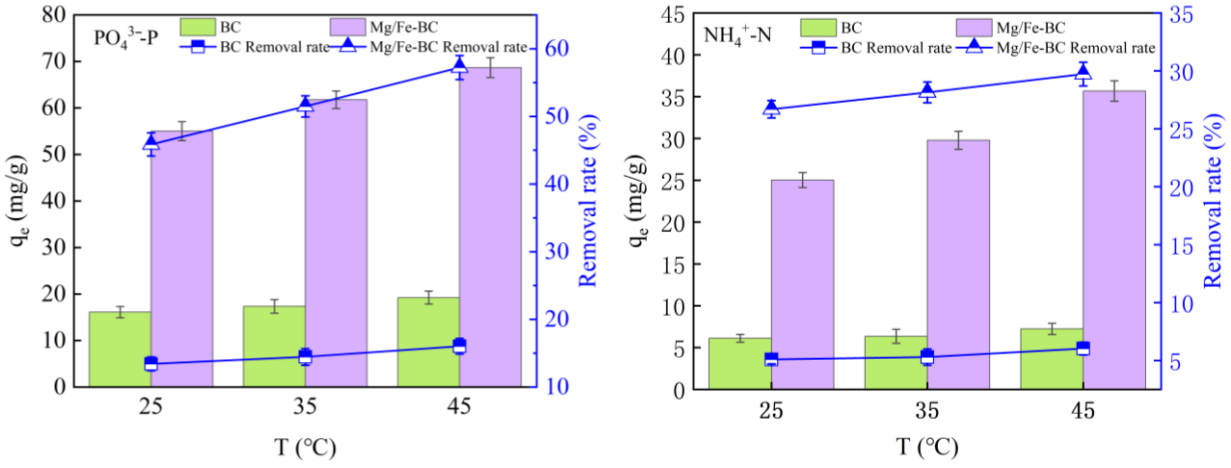


Figure 3. Adsorption capacity and removal rate of Mg/Fe-BC for PO_4^{3-}-P and NH_4^+-N in a single aqueous solution.

3.3. Adsorption of PO_4^{3-}-P and NH_4^+-N in Mixed Solutions by Mg/Fe-BC

3.3.1. Adsorption Kinetics

Comparative kinetic studies of PO_4^{3-}-P and NH_4^+-N adsorption elucidate distinct time-dependent removal patterns for the pollutant. The kinetic curves of PO_4^{3-}-P and NH_4^+-N adsorption by Mg/Fe-BC in mixed solutions are presented in Figure 4. During the initial adsorption stage (0–1 h), the PO_4^{3-}-P adsorption capacity of Mg/Fe-BC increased rapidly, followed by a slower uptake phase (1–4 h). After approximately 8 h, the adsorption reached equilibrium, indicating saturation of active sites. In contrast, NH_4^+-N adsorption exhibited a different kinetic profile: a sharp increase in capacity within 0–2 h, followed by a gradual rise (2–8 h) before stabilizing. Both PO_4^{3-}-P and NH_4^+-N adsorption capacities increased with prolonged contact time until all available binding sites were occupied. Notably, the adsorption rate of PO_4^{3-}-P was faster than that of NH_4^+-N, suggesting that NH_4^+-N removal was not solely governed by struvite precipitation but likely involved additional mechanisms such as pore filling and electrostatic attraction [32].

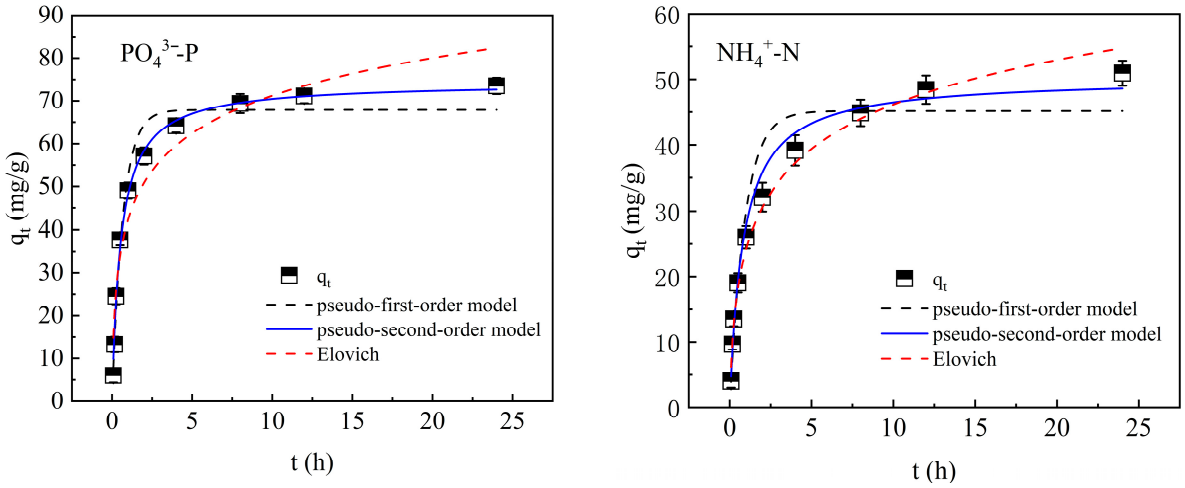


Figure 4. The adsorption kinetics model of PO_4^{3-}-P and NH_4^+-N by Mg/Fe-BC in the mixed solution.

Table 3 summarizes the kinetic fitting parameters for PO_4^{3-}-P and NH_4^+-N adsorption by Mg/Fe-BC. Compared to the pseudo-first-order (R^2 = 0.9732, 0.9471) and Elovich (R^2 = 0.9286, 0.9198) models, the adsorption behavior aligned more closely with the pseudo-second-order kinetic model (R^2 > 0.98), This indicates that the pseudo-second-order model is more suitable for simulating the adsorption processes of both PO_4^{3-}-P and NH_4^+-N. Previous studies have reported that the removal of PO_4^{3-}-P and NH_4^+-N is primarily driven by chemisorption mechanisms involving ion exchange, where the active sites on modified biochar surfaces participate in ion exchange with NH_4^+ or PO_4^{3-}, thereby forming covalent bonds or new compounds [33]. This process may involve the combined effects of surface precipitation and ligand exchange to facilitate the capture of PO_4^{3-}-P or NH_4^+-N by Mg/Fe-BC. The adsorption process in mixed solutions is influenced by multiple factors, with concomitant physisorption occurring through electrostatic attraction and external mass transfer processes [34]. Therefore, it can be inferred that the adsorption processes of PO_4^{3-}-P and NH_4^+-N in mixed solutions encompass both chemical reactions and physical adsorption.

Table 3. Adsorption kinetics parameters for Mg/Fe-BC.

Adsorption Kinetic Model		PO_4^{3-}-P	NH_4^+-N
Pseudo-first-order	q_e (mg/g)	67.88	45.16
	K_1(min^{-1})	1.48	1.09
	R^2	0.97	0.95
Pseudo-second-order	q_e (mg/g)	74.27	50.22
	K_2 (g/(mg·min))	0.02	0.02
	R^2	0.99	0.99
Elovich	α	336.16	103.77
	β	0.08	0.10
	R^2	0.93	0.92

3.3.2. Adsorption Isotherm

To further clarify the adsorption behavior of Mg/Fe-BC for PO_4^{3-}-P and NH_4^+-N under different temperature conditions, the Langmuir model and the Freundlich model were used to fit the experimental adsorption data. As shown in Figure 5, the adsorption amount of Mg/Fe-BC for PO_4^{3-}-P and NH_4^+-N increased with the increase in concentration until reaching the equilibrium stage. At low concentrations, the adsorption amount increased rapidly, but at high concentrations, the growth rate slowed down. Meanwhile, the adsorption amounts of both PO_4^{3-}-P and NH_4^+-N increased with the increase in temperature, among which the influence of temperature on the adsorption capacity of NH_4^+-N was obvious, while the adsorption effect of PO_4^{3-}-P on temperature was not sufficiently sensitive, which was consistent with the previous research results [31,32].

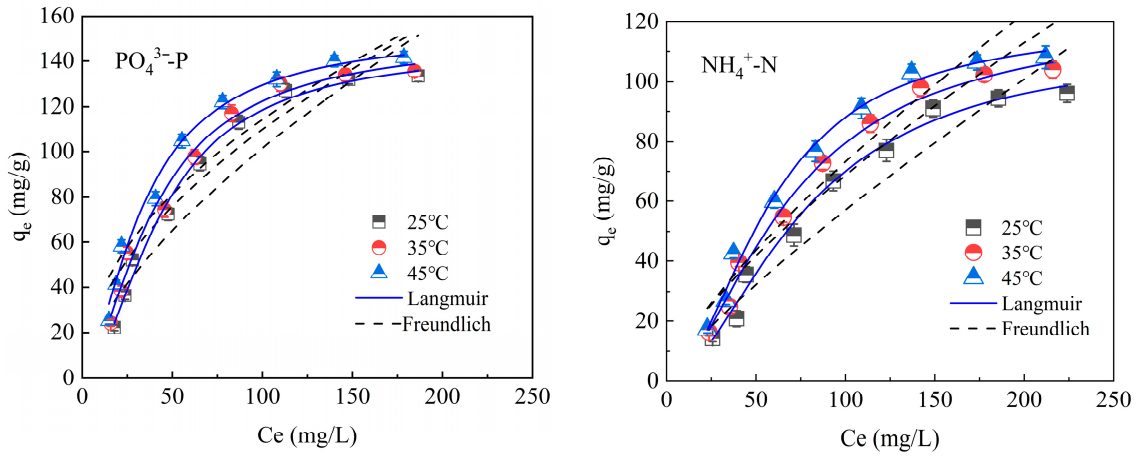


Figure 5. The adsorption isotherm model of PO_4^{3-}-P and NH_4^+-N by Mg/Fe-BC in the mixed solution.

The fitting parameters are shown in Table 4. The correlation coefficients R^2 of the Langmuir model for the adsorption behaviors of PO_4^{3-}-P and NH_4^+-N are all higher than those of the Freundlich model. This seems to indicate that the adsorption process of Mg/Fe-BC on PO_4^{3-}-P and NH_4^+-N is an idealized monolayer adsorption. However, after modification, Mg/Fe-BC has multiple substances such as Mg/Fe-LDH, iron oxides, and magnesium oxides on its pore surface, and the correlation coefficient R^2 of the Freundlich model is higher than 0.91. Multilayer adsorption may also occur on heterogeneous surfaces. The surface of this dual-metal modified biochar has considerable adsorption active sites. Previous studies have reported that the dual-metal modified biochar may have multiple mechanisms for control, and the surface functional groups may serve as potential adsorption sites for electrostatic attraction [31,33]. The fitting parameters of the Langmuir model

show that the maximum capacity of Mg/Fe-BC for PO_4^{3-}-P is 145.97–153.05 mg/g, and the maximum adsorption capacity for NH_4^+-N is 112.63–121.51 mg/g. These results confirm that the introduction of magnesium-iron dual metals enhances the adsorption capacity of PO_4^{3-}-P and NH_4^+-N, and the adsorption effect is higher than that of some adsorbents in previous studies (Table 5). Moreover, the KF constants for PO_4^{3-}-P adsorption described by the Freundlich model are all greater than those for NH_4^+-N adsorption, indicating that the affinity of Mg/Fe-BC for PO_4^{3-}-P is significantly higher than that of NH_4^+-N. The 1/n value is lower than 0.85, which also reveals that there is chemical adsorption on the Mg/Fe-BC surface [31].

Table 4. Adsorption isotherm parameters for the Mg/Fe-BC.

Index	T	Langmuir			Freundlich		
		K_L (L/mg)	q_m (mg/g)	R^2	K_F	1/n	R^2
PO_4^{3-}-P	25 °C	0.01	145.97	0.99	5.28	0.64	0.92
	35 °C	0.03	150.39	0.98	9.28	0.54	0.91
	45 °C	0.04	153.05	0.98	11.85	0.49	0.91
NH_4^+-N	25 °C	0.04	112.63	0.98	2.37	0.75	0.92
	35 °C	0.04	119.60	0.99	1.29	0.82	0.94
	45 °C	0.07	123.51	0.99	2.53	0.72	0.93

Table 5. Mg/Fe-BC comparison of the maximum adsorption capacity with other adsorbents for PO_4^{3-}-P and NH_4^+-N.

Adsorbent	Target Pollutant Ions	Adsorption Capacity (mg/g)	Reference
Biochar derived from iron-rich sludge	PO_4^{3-}-P	1.83	[35]
Mg-alginate modified biochar	PO_4^{3-}-P	46.56	[36]
NBC, NMBC	NH_4^+-N	13.59, 23.78	[37]
MPB	NH_4^+-N	30.00	[38]
CA-MB	PO_4^{3-}-P, NH_4^+-N	31.80, 10.15	[32]
Fe-modified biochar	PO_4^{3-}-P, NH_4^+-N	26.14, 11.68	[39]
Mg-loaded biochar	PO_4^{3-}-P, NH_4^+-N	31.15, 24.04	[40]
Mg/Fe-BC	PO_4^{3-}-P, NH_4^+-N	145.97, 112.63	This work

3.4. Factors Influencing Simultaneous PO_4^{3-}-P and NH_4^+-N Adsorption by Mg/Fe-BC

3.4.1. Dosage

The effect of varying Mg/Fe-BC dosages on simultaneous PO_4^{3-}-P and NH_4^+-N adsorption is shown in Figure 6. With increasing Mg/Fe-BC dosage, the equilibrium adsorption capacity for PO_4^{3-}-P initially increased and then decreased, while NH_4^+-N adsorption exhibited a similar trend. The removal rate of both PO_4^{3-}-P and NH_4^+-N gradually increased with dosage before eventually stabilizing. The enhanced removal efficiencies of both PO_4^{3-}-P and NH_4^+-N can be ascribed to the dosage-dependent increase in available adsorption sites on Mg/Fe-BC surfaces [41]. At lower dosages, the limited adsorption capacity was constrained by insufficient active sites for pollutant binding. As the dosage increased further, the equilibrium adsorption capacity gradually decreased due to reduced concentrations of PO_4^{3-}-P and NH_4^+-N in solution, which lowered the probability of their interaction with Mg/Fe-BC [32]. At the optimal dosage of 3 g/L, maximum adsorption capacities were achieved at 92.69 mg/g (PO_4^{3-}-P) and 58.45 mg/g (NH_4^+-N), corresponding to removal efficiencies of 77.24% and 47.21%, respectively. Therefore, 3 g/L

was identified as the optimum dosage for simultaneous PO_4^{3-}-P and NH_4^+-N adsorption under these experimental conditions, providing a valuable reference for subsequent studies.

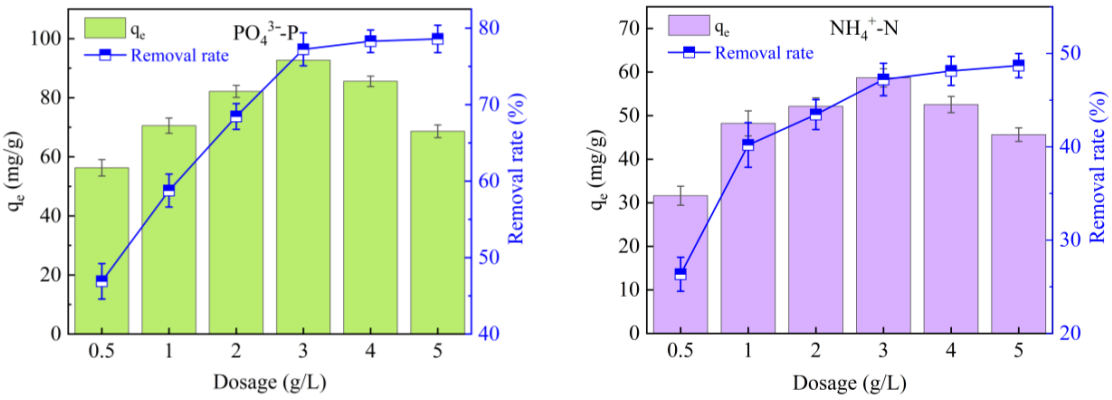


Figure 6. The influence of Mg/Fe-BC dosage on PO_4^{3-}-P and NH_4^+-N adsorption.

3.4.2. Initial pH

pH is one of the critical factors influencing the removal of contaminants by adsorbents. The existence forms of P and N in the aqueous solution at different pH values are shown in Figure S1. When pH = 1–4.7, the main forms of phosphorus are H_3PO_4 and $H_2PO_4^-$; when pH = 4.7–9.7, the main forms of phosphorus are $H_2PO_4^-$ and HPO_4^{2-}; and when pH = 9.7–14, HPO_4^{2-} and PO_4^{3-} are the dominant species. The dissociation constant of NH_4^+ is pKa = 9.25. When pH < 7, the main form of nitrogen in the aqueous solution is NH_4^+; when pH = 7–11.5, the main form of nitrogen is NH_4^+ and NH_3; and when pH > 11.5, free NH_3 is the dominant species. As shown in Figure 7, within the pH range of 3–9, the removal efficiencies of PO_4^{3-}-P and NH_4^+-N increased, accompanied by a slight rise in equilibrium adsorption capacity. Notably, the optimal pH range of 8–9 facilitated the removal of both PO_4^{3-}-P and NH_4^+-N, as struvite crystallization is most favorable at approximately pH 8.5 [42]. However, when the pH exceeded 9, the adsorption capacity for PO_4^{3-}-P significantly decreased. This decline can be attributed to the solution pH approaching the point of zero charge (pH_{pzc} = 8.82) of Mg/Fe-BC, leading to a reduction in the positive surface charge of the modified biochar and intensified competition between hydroxyl ions (OH^-) and phosphate ions (PO_4^{3-}) [43,44]. In contrast, NH_4^+-N adsorption remained relatively stable at pH 9–10 but experienced a sharp decline in removal efficiency at pH 11. This phenomenon likely results from the conversion of NH_4^+ to NH_3 under highly alkaline conditions [43]. The highest adsorption performance for both phosphate and ammonium was consistently observed at pH 8–9, further confirming the significant role of struvite formation in NH_4^+-N adsorption under weakly alkaline conditions.

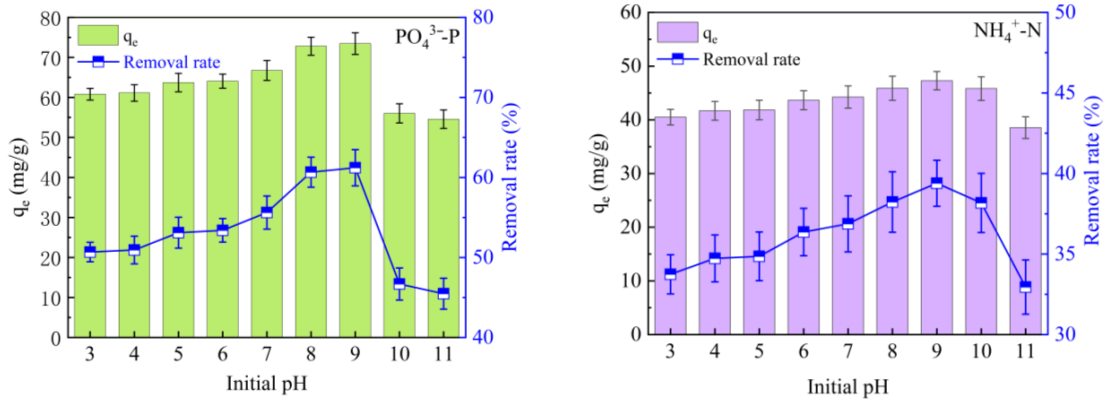


Figure 7. The influence of initial pH on PO_4^{3-}-P and NH_4^+-N adsorption.

3.4.3. Coexisting Ions

In practical biogas slurry, various coexisting ions may potentially interfere with the adsorption of PO_4^{3-}-P and NH_4^+. As shown in Figure 8, the presence of Na^+ at different concentrations had relatively minor effects on the simultaneous adsorption of PO_4^{3-}-P and NH_4^+, while K^+ and Ca^{2+} significantly affected their equilibrium adsorption capacities. On the one hand, K^+ reacts with PO_4^{3-}-P and trace amounts of Mg^{2+} in Mg/Fe-BC to form $MgKPO_4 \cdot nH_2O$; on the other hand, Ca^{2+} can also react with PO_4^{3-}-P to form phosphate byproducts such as $Ca_{10}(PO_4)_6(OH)_2$ that inhibit struvite crystallization [45]. For NH_4^+-N removal, Ca^{2+} affects the cation exchange capacity between Mg/Fe-BC and NH_4^+-N, thereby reducing the adsorption capacity of Mg/Fe-BC for NH_4^+-N. The effects of anions showed that Cl^- and NO_3^- had relatively small impacts on the simultaneous adsorption of PO_4^{3-}-P and NH_4^+; HCO_3^- appears to competitively occupy the adsorption sites for both PO_4^{3-}-P and NH_4^+-N, which is consistent with previous research reports [2]. Moreover, higher concentrations of HCO_3^- can increase the solution pH, leading to additional competition from hydroxide ions [46]. Therefore, when using Mg/Fe-BC to adsorb PO_4^{3-}-P and NH_4^+, the factors of competitive adsorption must be fully considered.

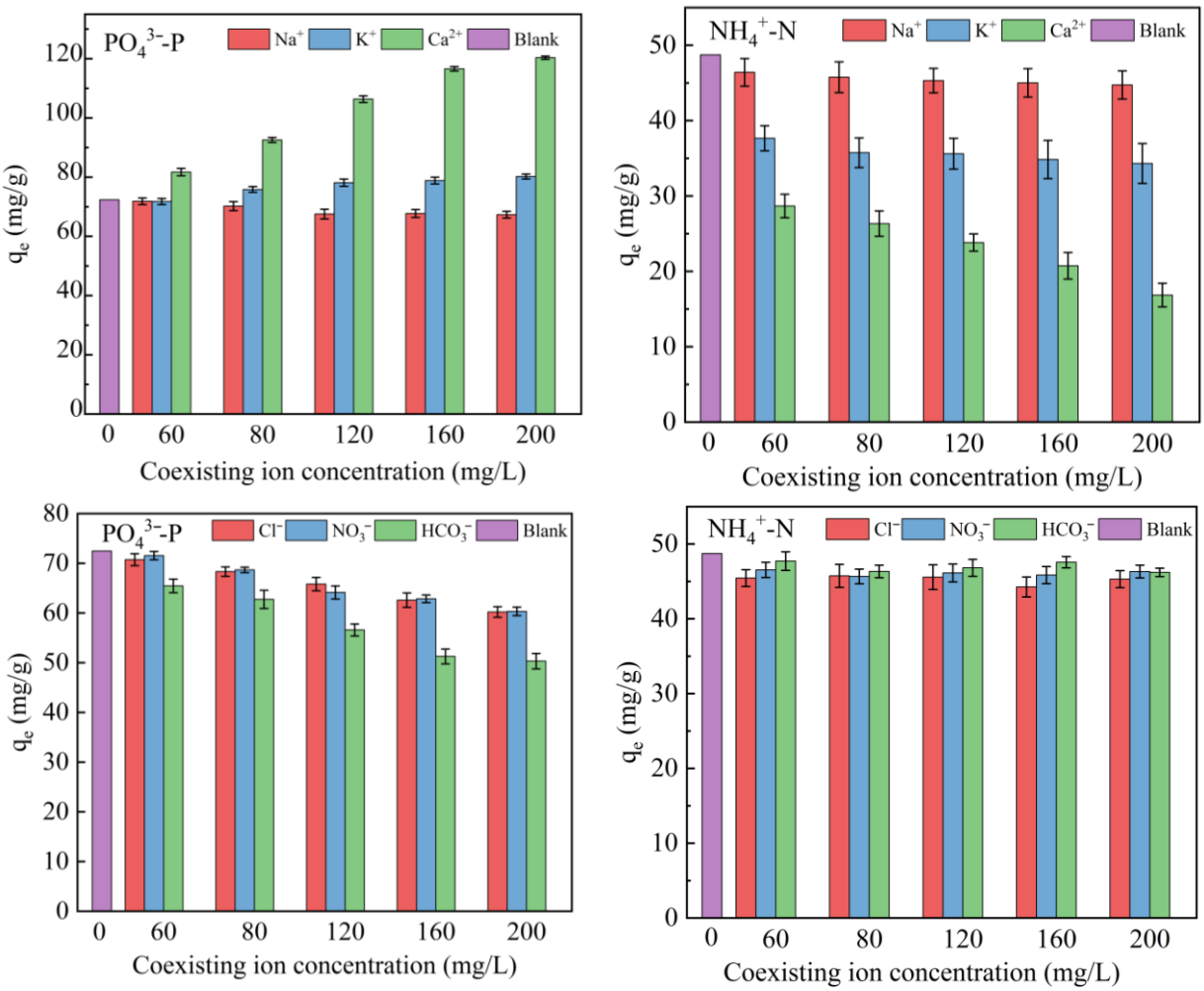


Figure 8. The influence of coexisting ions on PO_4^{3-}-P and NH_4^+-N adsorption.

3.5. Adsorption Performance of Mg/Fe-BC in Chicken Manure Biogas Slurry

3.5.1. The Influence of Dosage on the Adsorption of PO_4^{3-}-P and NH_4^+-N

In previous sections, we investigated the adsorption characteristics of Mg/Fe-BC at different dosages in simulated aqueous solutions, where 3 g/L of Mg/Fe-BC achieved the

highest removal rates for PO_4^{3-} and NH_4^+. However, in actual chicken manure biogas slurry (PO_4^{3-}-P: 32.86 mg/L; NH_4^+-N: 1279.45 mg/L), the adsorption environment is significantly more complex than in simulated solutions. Consequently, Mg/Fe-BC dosage emerged as a critical operational parameter governing the adsorption efficiency of both PO_4^{3-} and NH_4^+ in biogas slurry treatment systems. Figure 9 demonstrated a characteristic saturation curve for PO_4^{3-}-P removal, where the efficiency exhibited rapid enhancement from 3 to 10 g/L Mg/Fe-BC dosage (reaching 83.65%), followed by asymptotic stabilization (86.86% at 30 g/L). For NH_4^+-N adsorption in biogas slurry, within the dosage range of 3–15 g/L, the removal rate surged to 32.77%. When the dosage was increased to 30 g/L, the NH_4^+-N removal rate reached 36.86%. Compared to the simulated solution, Mg/Fe-BC maintained considerable removal efficiency for PO_4^{3-} and NH_4^+ in biogas slurry with high initial concentrations. Similar results were reported by Chung et al., who observed a positive correlation between initial concentration and equilibrium adsorption capacity when the N/P ratio exceeded 5:1 [47]. Thus, the adsorption process of Mg/Fe-BC may also involve synergistic effects.

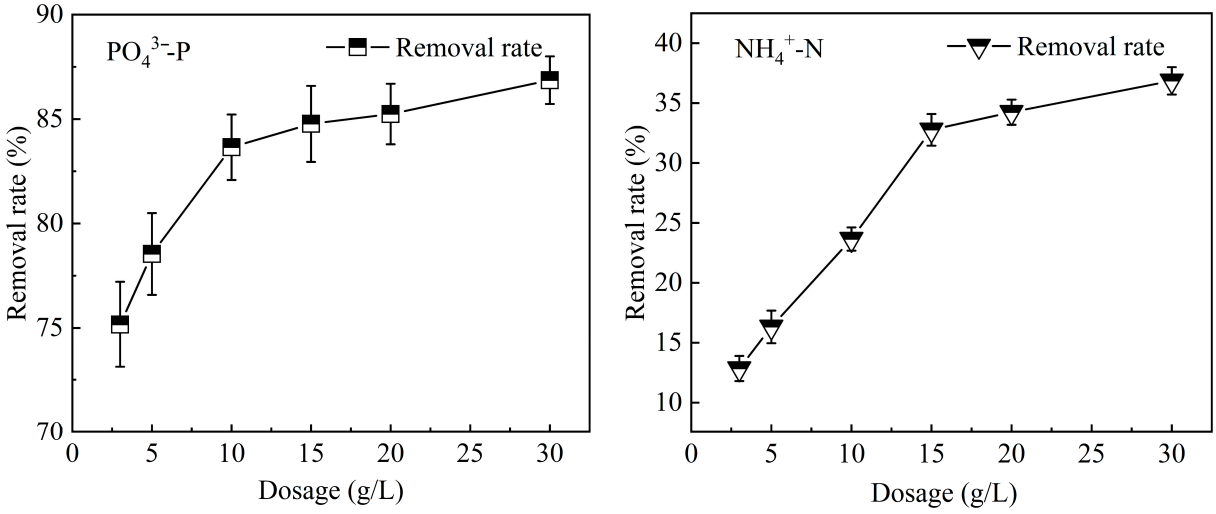


Figure 9. The influence of dosage on the removal rates of PO_4^{3-}-P and NH_4^+-N in chicken manure biogas slurry.

3.5.2. Effect of Contact Time on PO_4^{3-}-P and NH_4^+-N Adsorption

Using 3 g/L of Mg/Fe-BC in chicken manure biogas slurry, the adsorption process was investigated. As shown in Figure 10, the PO_4^{3-}-P adsorption exhibited a rapid initial phase followed by slower uptake, eventually reaching equilibrium within 4 h, with the PO_4^{3-}-P concentration decreasing to 9.96 mg/L. The NH_4^+-N adsorption followed a similar trend, though requiring slightly longer to reach equilibrium, achieving a concentration of 1142.76 mg/L after 4 h. Both adsorption processes followed the pseudo-second-order kinetic model, with fitted correlation coefficients $R^2 > 0.99$, confirming chemisorption as the dominant mechanism. Typically, increasing adsorbent dosage leads to progressive pollutant removal until the adsorbent reaches saturation, maximizing contaminant elimination [48]. The kinetic curves demonstrated that when PO_4^{3-}-P adsorption reached equilibrium, NH_4^+ adsorption simultaneously equilibrated, with removal rates of 75.14% and 12.8% respectively. As previously discussed, increasing dosage enhances adsorption capacities for both PO_4^{3-}-P and NH_4^+-N, primarily due to magnesium ammonium phosphate ($MgNH_4PO_4 \cdot 6H_2O$) formation as the main adsorption contributor. Additionally, at high N/P ratios, NH_4^+ adsorption involves independent mechanisms [46]. In conclusion, the highest synergistic removal efficiency for PO_4^{3-}-P and NH_4^+-N was achieved at a Mg/Fe-BC dosage of 30 g/L.

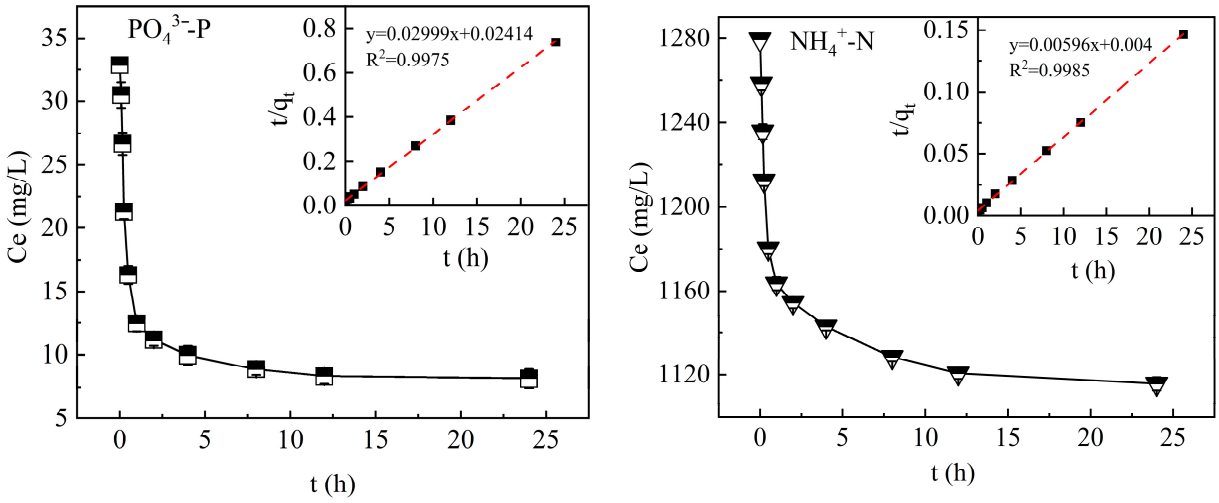


Figure 10. The influence of contact time on the equilibrium concentrations of PO_4^{3-}-P and NH_4^+-N in chicken manure biogas slurry.

3.6. Regeneration Experiment

The regeneration adsorption of PO_4^{3-}P and NH_4^+-N by Mg/Fe-BC is crucial for expanding its application in water treatment. As can be seen from Figure 11, after 5 cycles of adsorption, the removal rates of PO_4^{3-}P and NH_4^+-N in chicken manure biogas slurry by Mg/Fe-BC still reached 71.94% and 27.76% respectively. After the third cycle, the removal capacity significantly decreased, while the 4–5 cycles maintained a relatively stable state. This indicates that Mg/Fe-BC has a high recovery capacity for P and N in chicken manure biogas slurry, and it can still be regenerated after 5 cycles of adsorption.

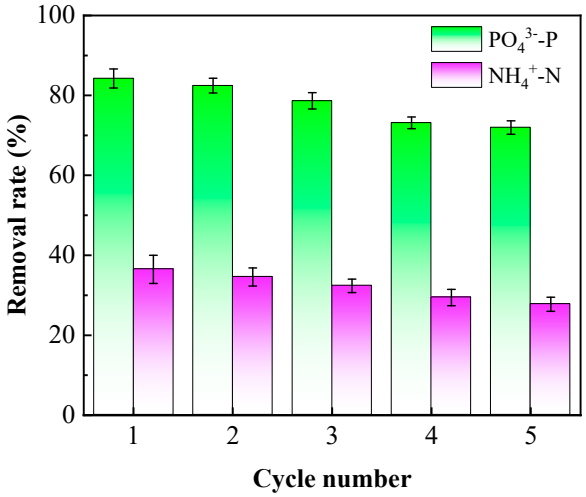


Figure 11. Regeneration experiment of Mg/Fe-BC for adsorbing PO_4^3-P and NH_4^+-N.

3.7. Adsorption Mechanisms

To reveal the adsorption mechanisms of PO_4^{3-} and NH_4^+, SEM-EDS was used to characterize the physicochemical properties of Mg/Fe-BC after adsorption (Figure 12). The post-adsorption Mg/Fe-BC surface showed rough morphology with abundant particle deposition, irregular pore structures, and partial micropore blockage. More importantly, SEM-EDS mapping results (Figure 12) demonstrated uniform distribution of phosphorus and nitrogen elements on the Mg/Fe-BC surface, further confirming the successful adsorption of PO_4^{3-}-P and NH_4^+-N.

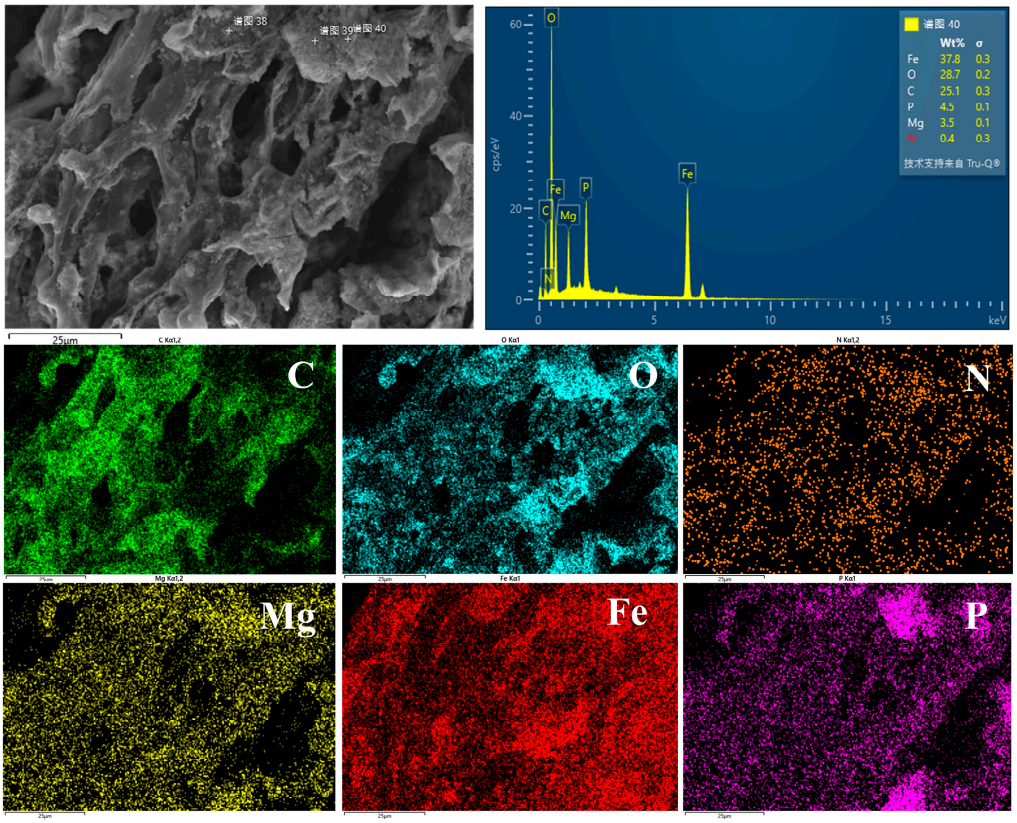


Figure 12. SEM-EDS images of Mg/Fe-BC after adsorbing PO_4^{3-}-P and NH_4^+-N.

The XPS spectra of Mg/Fe-BC after adsorbing PO_4^{3-}-P and NH_4^+-N are shown in Figure 13. In the C1s spectrum, the characteristic peak at 285.81 eV represents O-C-O, while the peak at 288.96 eV corresponds to O-C=O. The abundant oxygen-containing functional groups in Mg/Fe-BC facilitate its capture of PO_4^{3-} and NH_4^+ [49]. In the O1s spectrum, the peak at 530.45 eV mainly represents magnesium or iron oxides. Notably, the appearance of the P-O characteristic peak at 533.74 eV indicates PO_4^{3-}-P adsorption by Mg/Fe-BC [50]. The Mg1s spectrum displayed three characteristic peaks. The peak at 1304.30 eV primarily corresponds to struvite or Mg-O-P bonds, suggesting the formation of struvite or $Mg_3(PO_4)_2$ from Mg^{2+} with PO_4^{3-} and NH_4^+ [46]. The binding energies at 711.38 eV and 713.75 eV represent $Fe2p_3/_2$, while 724.48 eV represents $Fe2p_1/_2$, indicating iron oxides mainly containing Fe-O or Fe-OH bonds [21]. The P2p spectrum showed two characteristic peaks: P-O bond at 130.30 eV and Mg-O-P at 133.55 eV, demonstrating magnesium phosphate formation from magnesium ions and PO_4^{3-} [26]. In the N1s spectrum, the characteristic peak at 400.17 eV represents NH_4^+, while 403.57 eV corresponds to struvite or ammonium-containing compounds [46]. These results suggest that Mg^{2+} and NH_4^+-N mainly exist as struvite, while PO_4^{3-}-P primarily exists as magnesium/iron phosphates. Particularly when treating high-concentration biogas slurry, struvite precipitation serves as the main mechanism for ammonium and phosphate adsorption [26].

Therefore, the adsorption mechanisms of PO_4^{3-}-P on Mg/Fe-BC are attributed to electrostatic attraction, surface precipitation, and ligand exchange, whereas NH_4^+-N adsorption occurs primarily through physical adsorption, ion exchange, and electrostatic attraction [51]. In acidic environments, phosphate adsorption is governed by surface precipitation, electrostatic attraction, and ligand exchange [44], while ammonium adsorption is predominantly controlled by ion exchange [52,53]. Under alkaline conditions, surface precipitation becomes the dominant mechanism for phosphate removal, whereas electrostatic attraction plays the principal role in ammonium adsorption [26,54]. Since actual biogas

slurry exhibits weakly alkaline pH, the adsorption mechanisms of PO_4^{3-}-P and NH_4^+-N by Mg/Fe-BC are dominated by surface precipitation and electrostatic attraction, respectively.

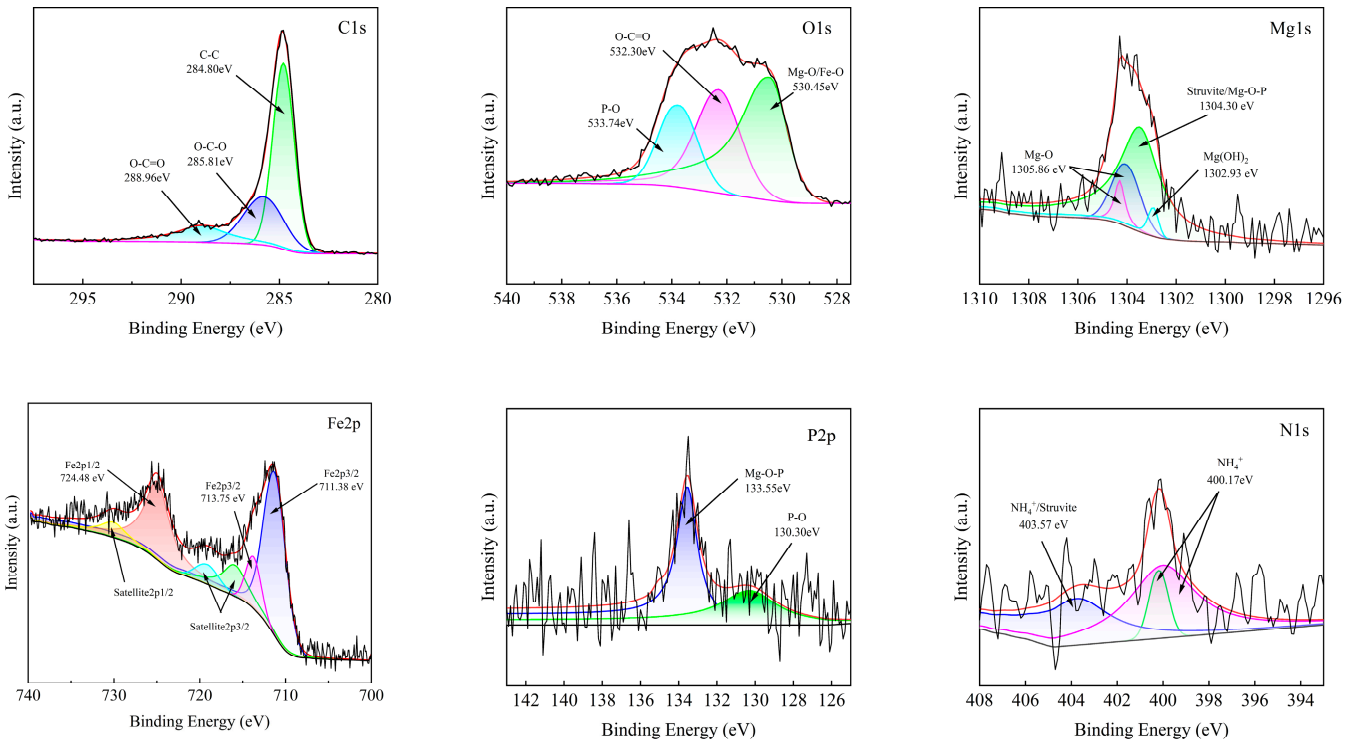


Figure 13. XPS spectra of Mg/Fe-BC after adsorbing PO_4^{3-}-P and NH_4^+-N.

4. Conclusions

This study prepared magnesium-iron layered double hydroxide modified biochar (Mg/Fe-BC) using the chemical co-precipitation method. Through characterization (SEM, BET, XRD, and FTIR) and adsorption experiments, the adsorption process, removal efficiency and mechanisms of phosphate and ammonium nitrogen by Mg/Fe-BC in simulated solutions or chicken manure biogas slurry were investigated. In single aqueous solutions containing 120 mg/L of either phosphate or ammonium nitrogen, the increase in temperature demonstrated a more significant enhancement in the adsorption capacity and removal efficiency of ammonium nitrogen compared to phosphate. The simultaneous adsorption of phosphate and ammonium nitrogen by Mg/Fe-BC followed the pseudo-second-order kinetic model and Langmuir isotherm model, indicating a monolayer chemisorption process. The maximum adsorption capacities reached 145.97–153.05 mg/g for phosphate and 112.63–121.51 mg/g for ammonium nitrogen. The optimal dosage for synergistic adsorption was determined to be 3 g/L. Within the pH range of 3–9, the adsorption of both phosphate and ammonium nitrogen was minimally affected. Among interfering ions, Ca^{2+} showed significant interference on both phosphate and ammonium nitrogen adsorption, while HCO_3^- particularly affected phosphate adsorption. For chicken manure biogas slurry treatment, the equilibrium adsorption capacities of Mg/Fe-BC reached 163.77 mg/g for phosphate and 32.49 mg/g for ammonium nitrogen. When the dosage increased to 30 g/L, the removal rates achieved 86.86% for phosphate and 36.86% for ammonium nitrogen. After 5 cycles of adsorption experiments, Mg/Fe-BC maintained a high removal rate for PO_4^3-P and NH_4^+-N. The adsorption mechanisms of PO_4^{3-}-P mainly rely on ligand exchange and electrostatic attraction. The removal process of NH_4^+-N is driven by ion exchange and hydrogen bonding. This study demonstrates that Mg/Fe-BC can serve as an

environmentally friendly and highly efficient adsorbent for the simultaneous recovery of phosphate and ammonium nitrogen from biogas slurry.

Supplementary Materials: The following supporting information can be downloaded at: https://www.mdpi.com/article/10.3390/pr13082504/s1, Text S1: adsorption capacity and removal rate equation; Text S2: the equations of pseudo-first-order model and pseudo-second-order model; Text S3: the equations of Langmuir model and Freundlich mode; Figure S1: speciation diagrams of P (a) and N (b) in aqueous media at various pH levels.

Author Contributions: Conceptualization: T.L. and J.L.; methodology: T.L. and J.L.; formal analysis and investigation: T.L., J.L. and Z.L.; preparation and characterization of modified biochar: T.L.; adsorption processes and their analysis: Z.L.; writing—original draft preparation: T.L. and J.L.; writing—review and editing: T.L. and J.L.; visualization: X.C.; resources: J.L. and X.C.; J.L. and X.C. All authors have read and agreed to the published version of the manuscript.

Funding: The authors would like to express their gratitude for the financial support provided by Gansu Major Science and Technology Project (22ZD6WA056) and Gansu Province Higher Education Industry Support and Guidance Project (2022CYZC-28) and Modern Silk Road Cold and Drought Agricultural Science and Technology Support Project (GSLK-2022-19) and Science and Technology Plan Project of Gannan (2023JY1SC002) and Jiuquan Science and Technology Support Program (2024CA1083).

Data Availability Statement: The original contributions presented in this study are included in this article. Further inquiries should be directed to the corresponding authors.

Acknowledgments: The author would like to express his sincere gratitude to the Lanzhou Institute of Chemical Physics, Chinese Academy of Sciences for the technical support provided for the characterization of the modified biochar. All individuals included in this section have consented to the acknowledgement.

Conflicts of Interest: The authors declare no conflicts of interest.

References

1. Yuan, Z.; Ji, J.; Sheng, H.; Jiang, S.; Chen, T.; Liu, X.; Liu, X.; Zhuang, Y.; Zhang, L. Animal Based Diets and Environment: Perspective from Phosphorus Flow Quantifications of Livestock and Poultry Raising in China. *J. Environ. Manag.* **2019**, *244*, 199–207. [CrossRef] [PubMed]
2. Yang, F.; Sui, L.; Tang, C.; Li, J.; Cheng, K.; Xue, Q. Sustainable Advances on Phosphorus Utilization in Soil via Addition of Biochar and Humic Substances. *Sci. Total Environ.* **2021**, *768*, 145106. [CrossRef] [PubMed]
3. Sajjad, M.; Huang, Q.; Khan, S.; Nawab, J.; Khan, M.A.; Ali, A.; Ullah, R.; Kubar, A.A.; Guo, G.; Yaseen, M.; et al. Methods for the Removal and Recovery of Nitrogen and Phosphorus Nutrients from Animal Waste: A Critical Review. *Ecol. Front.* **2024**, *44*, 2–14. [CrossRef]
4. Li, Y.; Wang, M.; Chen, X.; Cui, S.; Hofstra, N.; Kroeze, C.; Ma, L.; Xu, W.; Zhang, Q.; Zhang, F.; et al. Multi-Pollutant Assessment of River Pollution from Livestock Production Worldwide. *Water Res.* **2022**, *209*, 117906. [CrossRef] [PubMed]
5. Bhatnagar, N.; Ryan, D.; Murphy, R.; Enright, A.M. A Comprehensive Review of Green Policy, Anaerobic Digestion of Animal Manure and Chicken Litter Feedstock Potential–Global and Irish Perspective. *Renew. Sust. Energ. Rev.* **2022**, *154*, 111884. [CrossRef]
6. Huang, X.; Wang, S.; Shi, Z.; Fang, L.; Yin, C. Challenges and Strategies for Biogas Production in the Circular Agricultural Waste Utilization Model: A Case Study in Rural China. *Energy* **2022**, *241*, 122889. [CrossRef]
7. Duan, N.; Zhang, D.; Lin, C.; Zhang, Y.; Zhao, L.; Liu, H.; Liu, Z. Effect of Organic Loading Rate on Anaerobic Digestion of Pig Manure: Methane Production, Mass Flow, Reactor Scale and Heating Scenarios. *J. Environ. Manag.* **2019**, *231*, 646–652. [CrossRef] [PubMed]
8. Ke, L.; Liu, X.; Du, B.; Wang, Y.; Zheng, Y.; Li, Q. Component Analysis and Risk Assessment of Biogas Slurry from Biogas Plants. *Chin. J. Chem. Eng.* **2022**, *44*, 182–191. [CrossRef]
9. Wicker, R.; Bhatnagar, A. Application of Nordic Microalgal-Bacterial Consortia for Nutrient Removal from Wastewater. *Chem. Eng. J.* **2020**, *398*, 125567. [CrossRef]
10. Karri, R.R.; Sahu, J.N.; Chimmiri, V. Critical Review of Abatement of Ammonia from Wastewater. *J. Mol. Liq.* **2018**, *261*, 21–31. [CrossRef]

11. Ma, L.L.; Ma, C.; Zhang, H.F.; Wang, B.H. Identifying Influential Spreaders in Complex Networks Based on Gravity Formula. *Phys. A* **2016**, *451*, 205–212. [CrossRef]
12. Qiu, J.; Hou, H.; Liang, S.; Yang, L.; Gan, Q.; Tao, S.; Yu, W.; Lv, R.; Ding, L.; Xiao, K.; et al. Hierarchically Porous Biochar Preparation and Simultaneous Nutrient Recovery from Sewage Sludge via Three Steps of Alkali-Activated Pyrolysis, Water Leaching and Acid Leaching. *Resour. Conserv. Recycl.* **2022**, *176*, 105953. [CrossRef]
13. Zhu, Y.; Liu, S.; Chen, H.; Yu, P.; Chen, C. Evaluating Biochar for Adsorption of Ammonium Nitrogen in Wastewater: Insights into Modifications and Mechanisms. *Environ. Res.* **2025**, *277*, 121615. [CrossRef] [PubMed]
14. Fang, Y.; Ali, A.; Gao, Y.; Zhao, P.; Li, R.; Li, X.; Liu, J.; Luo, Y.; Peng, Y.; Wang, H.; et al. Preparation and Characterization of MgO Hybrid Biochar and Its Mechanism for High Efficient Recovery of Phosphorus from Aqueous Media. *Biochar* **2022**, *4*, 171. [CrossRef]
15. Cao, J.; Wang, R.; Zhu, H.; Cao, S.; Duan, Z. Effect of Fenton Pre-Oxidation on the Physicochemical Properties of Sludge-Based Biochar and Its Adsorption Mechanisms for Ammonia Nitrogen Removal. *J. Environ. Chem. Eng.* **2023**, *11*, 110689. [CrossRef]
16. Rybka, K.; Matusik, J.; Marzec, M. Mg/Al and Mg/Fe Layered Double Hydroxides Derived from Magnesite and Chemicals: The Effect of Adsorbent Features and Anions Chemistry on Their Removal Efficiency. *J. Clean. Prod.* **2022**, *332*, 130084. [CrossRef]
17. Fang, Q.; Ye, S.; Yang, H.; Yang, K.; Zhou, J.; Gao, Y.; Lin, Q.; Tan, X.; Yang, Z. Application of Layered Double Hydroxide-Biochar Composites in Wastewater Treatment: Recent Trends, Modification Strategies, and Outlook. *J. Hazard. Mater.* **2021**, *420*, 126569. [CrossRef]
18. Yang, H.; Ye, S.; Zeng, Z.; Zeng, G.; Tan, X.; Xiao, R.; Wang, J.; Song, B.; Du, L.; Qin, M.; et al. Utilization of Biochar for Resource Recovery from Water: A Review. *Chem. Eng. J.* **2020**, *397*, 125502. [CrossRef]
19. Li, H.; Wang, Y.; Zhao, Y.; Wang, L.; Feng, J.; Sun, F. Efficient Simultaneous Phosphate and Ammonia Adsorption Using Magnesium-Modified Biochar Beads and Their Recovery Performance. *J. Environ. Chem. Eng.* **2023**, *11*, 110875. [CrossRef]
20. Li, T.; Li, J.; Li, T.; Cheng, X. Characterization of Magnesium-Iron Modified Biochar to Alleviate Ammonia Inhibition and Enhance Anaerobic Digestion of Chicken Manure. *Waste Biomass Valorization* **2025**, *25*, 2894. [CrossRef]
21. Bian, H.; Wang, M.; Han, J.; Hu, X.; Xia, H.; Wang, L.; Fang, C.; Shen, C.; Man, Y.B.; Wong, M.H.; et al. MgFe-LDH@Biochars for Removing Ammonia Nitrogen and Phosphorus from Biogas Slurry: Synthesis Routes, Composite Performance, and Adsorption Mechanisms. *Chemosphere* **2023**, *324*, 138333. [CrossRef] [PubMed]
22. Li, L.; Qi, G.; Wang, B.; Yue, D.; Wang, Y.; Sato, T. Fulvic Acid Anchored Layered Double Hydroxides: A Multifunctional Composite Adsorbent for the Removal of Anionic Dye and Toxic Metal. *J. Hazard. Mater.* **2018**, *343*, 19–28. [CrossRef]
23. Bhatia, A.; Khatri, A.; Yadav, M.; Kumari, A.; Mona, S.; Bhateria, R. Potential of Iron Oxide Nanoparticles in Enhancing Growth and Development of Plants: A Review. *Physiol. Mol. Plant Pathol.* **2025**, *139*, 102746. [CrossRef]
24. Roy Choudhury, M.; Christopher, J.; Das, S.; Apan, A.; Menzies, N.W.; Chapman, S.; Mellor, V.; Dang, Y.P. Detection of Calcium, Magnesium, and Chlorophyll Variations of Wheat Genotypes on Sodic Soils Using Hyperspectral Red Edge Parameters. *Environ. Technol. Innov.* **2022**, *27*, 102469. [CrossRef]
25. Tan, W.T.; Zhou, H.; Tang, S.F.; Zeng, P.; Gu, J.F.; Liao, B.H. Enhancing Cd(II) Adsorption on Rice Straw Biochar by Modification of Iron and Manganese Oxides. *Environ. Pollut.* **2022**, *300*, 118899. [CrossRef] [PubMed]
26. Rahman, S.; Navarathna, C.M.; Krishna Das, N.; Alchouron, J.; Reneau, P.; Stokes, S.; Thirumalai, R.V.K.G.; Perez, F.; Barbary Hassan, E.; Mohan, D. High Capacity Aqueous Phosphate Reclamation Using Fe/Mg-Layered Double Hydroxide (LDH) Dispersed on Biochar. *J. Colloid Interface Sci.* **2021**, *597*, 182–195. [CrossRef]
27. Liu, H.; Shan, J.; Chen, Z.; Lichtfouse, E. Efficient Recovery of Phosphate from Simulated Urine by Mg/Fe Bimetallic Oxide Modified Biochar as a Potential Resource. *Sci. Total Environ.* **2021**, *784*, 147546. [CrossRef]
28. Fang, L.; Li, J.S.; Donatello, S.; Cheeseman, C.R.; Poon, C.S.; Tsang, D.C.W. Use of Mg/Ca Modified Biochars to Take Up Phosphorus from Acid-Extract of Incinerated Sewage Sludge Ash (ISSA) for Fertilizer Application. *J. Clean. Prod.* **2020**, *244*, 118853. [CrossRef]
29. Li, X.; Shi, J. Simultaneous Adsorption of Tetracycline, Ammonium and Phosphate from Wastewater by Iron and Nitrogen Modified Biochar: Kinetics, Isotherm, Thermodynamic and Mechanism. *Chemosphere* **2022**, *293*, 133574. [CrossRef]
30. Cheng, H.; Zhu, Q.; Xing, Z. Adsorption of Ammonia Nitrogen in Low Temperature Domestic Wastewater by Modification Bentonite. *J. Clean. Prod.* **2019**, *233*, 720–730. [CrossRef]
31. Jia, Z.; Zeng, W.; Xu, H.; Li, S.; Peng, Y. Adsorption Removal and Reuse of Phosphate from Wastewater Using a Novel Adsorbent of Lanthanum-Modified Platanus Biochar. *Process Saf. Environ.* **2020**, *140*, 221–232. [CrossRef]
32. Feng, Q.; Chen, M.; Wu, P.; Zhang, X.; Wang, S.; Yu, Z.; Wang, B. Simultaneous Reclaiming Phosphate and Ammonium from Aqueous Solutions by Calcium Alginate-Biochar Composite: Sorption Performance and Governing Mechanisms. *Chem. Eng. J.* **2022**, *429*, 132166. [CrossRef]
33. Wang, C.; Zhou, Y.; Yu, F.; Zhu, X.; Dong, M.; Li, Q. Recovery of Phosphate from Aqueous Solution by Modified Biochar with Concentrated Seawater and Its Potential Application as Fertilizer. *J. Environ. Chem. Eng.* **2024**, *12*, 112646. [CrossRef]

34. Yang, X.; Yang, F.; Liu, C.; Sun, H.; Hou, D.; Zheng, Y.; Gao, H.; Shi, R.; He, X.; Lin, X. Adsorption Characteristics and Mechanism Insights of K_2FeO_4 Coupling with $ZnCl_2$-Assisted Modified Functionalized Biochar for Pb (II) in Wastewater. *J. Environ. Chem. Eng.* **2025**, *13*, 115279. [CrossRef]
35. Wang, Z.; Li, Y.; Xie, X.; Wang, Z. Bifunctional $MnFe_2O_4$/Chitosan Modified Biochar Composite for Enhanced Methyl Orange Removal Based on Adsorption and Photo-Fenton Process. *Colloids Surf. A* **2021**, *613*, 126104. [CrossRef]
36. Cui, X.; Dai, X.; Khan, K.Y.; Li, T.; Yang, X.; He, Z. Removal of Phosphate from Aqueous Solution Using Magnesium-Alginate/Chitosan Modified Biochar Microspheres Derived from Thalia Dealbata. *Bioresour. Technol.* **2016**, *218*, 1123–1132. [CrossRef]
37. Tan, M.; Li, Y.; Chi, D.; Wu, Q. Efficient Removal of Ammonium in Aqueous Solution by Ultrasonic Magnesium-Modified Biochar. *Chem. Eng. J.* **2023**, *461*, 142072. [CrossRef]
38. Gong, Y.P.; Ni, Z.Y.; Xiong, Z.Z.; Cheng, L.H.; Xu, X.H. Phosphate and Ammonium Adsorption of the Modified Biochar Based on Phragmites Australis after Phytoremediation. *Environ. Sci. Pollut. R.* **2017**, *24*, 8326–8335. [CrossRef]
39. Li, B.; Jing, F.; Hu, Z.; Liu, Y.; Xiao, B.; Guo, D. Simultaneous Recovery of Nitrogen and Phosphorus from Biogas Slurry by Fe-Modified Biochar. *J. Saudi Chem. Soc.* **2021**, *25*, 101213. [CrossRef]
40. Jiang, Y.H.; Li, A.Y.; Deng, H.; Ye, C.H.; Wu, Y.Q.; Linmu, Y.D.; Hang, H.L. Characteristics of Nitrogen and Phosphorus Adsorption by Mg-Loaded Biochar from Different Feedstocks. *Bioresour. Technol.* **2019**, *276*, 183–189. [CrossRef]
41. Luo, L.; Wang, G.; Shi, G.; Zhang, M.; Zhang, J.; He, J.; Xiao, Y.; Tian, D.; Zhang, Y.; Deng, S.; et al. The Characterization of Biochars Derived from Rice Straw and Swine Manure, and Their Potential and Risk in N and P Removal from Water. *J. Environ. Manag.* **2019**, *245*, 1–7. [CrossRef] [PubMed]
42. Moulessehoul, A.; Gallart-Mateu, D.; Harrache, D.; Djaroud, S.; de la Guardia, M.; Kameche, M. Conductimetric Study of Struvite Crystallization in Water as a Function of pH. *J. Cryst. Growth* **2017**, *471*, 42–52. [CrossRef]
43. Li, R.; Wang, J.J.; Zhou, B.; Zhang, Z.; Liu, S.; Lei, S.; Xiao, R. Simultaneous Capture Removal of Phosphate, Ammonium and Organic Substances by MgO Impregnated Biochar and Its Potential Use in Swine Wastewater Treatment. *J. Clean. Prod.* **2017**, *147*, 96–107. [CrossRef]
44. Shin, J.; Rho, H.; Cho, Y.; Son, C.; Kwak, J.; Kim, S.; Ki, S.; Kim, H.J.; Lee, Y.-G.; Park, Y.; et al. Functionalization of Coffee Waste Biochars with Ca/Fe Layered Double Hydroxides for Enhanced Removal and Selectivity of Phosphate Ions: Mechanisms and Reusability. *J. Water Process. Eng.* **2025**, *76*, 108123. [CrossRef]
45. Yan, H.; Shih, K. Effects of Calcium and Ferric Ions on Struvite Precipitation: A New Assessment Based on Quantitative X-Ray Diffraction Analysis. *Water Res.* **2016**, *95*, 310–318. [CrossRef] [PubMed]
46. Cai, G.; Ye, Z.L. Concentration-Dependent Adsorption Behaviors and Mechanisms for Ammonium and Phosphate Removal by Optimized Mg-Impregnated Biochar. *J. Clean. Prod.* **2022**, *349*, 131453. [CrossRef]
47. Chung, H.K.; Kim, W.H.; Park, J.; Cho, J.; Jeong, T.Y.; Park, P.K. Application of Langmuir and Freundlich Isotherms to Predict Adsorbate Removal Efficiency or Required Amount of Adsorbent. *J. Ind. Eng. Chem.* **2015**, *28*, 241–246. [CrossRef]
48. Pan, F.; Wei, H.; Huang, Y.; Song, J.; Gao, M.; Zhang, Z.; Teng, R.; Jing, S. Phosphorus Adsorption by Calcium Chloride-Modified Buckwheat Hulls Biochar and the Potential Application as a Fertilizer. *J. Clean. Prod.* **2024**, *444*, 141233. [CrossRef]
49. Lou, L.; Li, W.; Yao, H.; Luo, H.; Liu, G.; Fang, J. Corn Stover Waste Preparation Cerium-Modified Biochar for Phosphate Removal from Pig Farm Wastewater: Adsorption Performance and Mechanism. *Biochem. Eng. J.* **2024**, *212*, 109530. [CrossRef]
50. Wang, B.; Hu, X.; Li, L.; Wang, H.; Huang, H.; Wang, R.; Zhou, D.; Yuan, J.; Chen, L. Application and Functionalization of Toxic Waste Sludge-Derived Biochar for Efficient Phosphate Separation from Aqueous Media: Toxicity Diminution, Robust Adsorption, and Inner Mechanism. *Chem. Eng. J.* **2023**, *468*, 143745. [CrossRef]
51. Tang, Y.; Alam, M.S.; Konhauser, K.O.; Alessi, D.S.; Xu, S.; Tian, W.; Liu, Y. Influence of Pyrolysis Temperature on Production of Digested Sludge Biochar and Its Application for Ammonium Removal from Municipal Wastewater. *J. Clean. Prod.* **2019**, *209*, 927–936. [CrossRef]
52. Luo, Y.; Xie, K.; Feng, Y.; He, Q.; Zhang, K.; Shen, S.; Wang, F. Synthesis of a $La(OH)_3$ Nanorod/Walnut Shell Biochar Composite for Reclaiming Phosphate from Aqueous Solutions. *Colloid Surf. A* **2021**, *610*, 125736. [CrossRef]
53. Cichy, B.; Kuzdzal, E.; Krzton, H. Phosphorus Recovery from Acidic Wastewater by Hydroxyapatite Precipitation. *J. Environ. Manag.* **2019**, *232*, 421–427. [CrossRef] [PubMed]
54. He, D.; Yang, R.; Fu, Y.; Zhu, B. Superior Properties of Biochar Contribute to Soil Carbon Sequestration and Climate Change Mitigation. *J. Environ. Chem. Eng.* **2025**, *13*, 116936. [CrossRef]

Disclaimer/Publisher's Note: The statements, opinions and data contained in all publications are solely those of the individual author(s) and contributor(s) and not of MDPI and/or the editor(s). MDPI and/or the editor(s) disclaim responsibility for any injury to people or property resulting from any ideas, methods, instructions or products referred to in the content.